The Journal of Immunology

Differential Segmental Flexibility and Reach Dictate the Antigen Binding Mode of Chimeric IgD and IgM: Implications for the Function of the B Cell Receptor

Geir Å. Løset, Kenneth H. Roux, Ping Zhu, Terje E. Michaelsen and Inger Sandlie

J Immunol 2004; 172:2925-2934; ;
doi: 10.4049/jimmunol.172.5.2925
http://www.jimmunol.org/content/172/5/2925

The Journal of Immunology is published twice each month by
The American Association of Immunologists, Inc.,
9650 Rockville Pike, Bethesda, MD 20814-3994.

Print ISSN: 0022-1767 Online ISSN: 1550-6606.

Differential Segmental Flexibility and Reach Dictate the Antigen Binding Mode of Chimeric IgD and IgM: Implications for the Function of the B Cell Receptor[1]

Geir Å. Løset,[2]* Kenneth H. Roux,[†] Ping Zhu,[†] Terje E. Michaelsen,[‡] and Inger Sandlie*

Mature, naive B cells coexpress IgD and IgM with identical binding sites. In this study, the binding properties of such IgM and IgD are compared to determine how size and shape may influence their ability to bind Ag and thus function as receptors. To dissect their intrinsic binding properties, recombinant IgM and IgD were produced in soluble form as monomers of the basic H_2L_2 Ab architecture, each with two Ag binding sites. Since these sites are connected with a hinge region in IgD and structural Ig domains in IgM, the two molecules differ significantly in this region. The results show that IgD exhibited the larger angle and longer distance between its binding sites, as well as having the greater flexibility. Relative functional affinity was assessed on two antigenic surfaces with high or low epitope density, respectively. At high epitope density, IgM had a higher functional affinity for the Ag compared with IgD. The order was reversed at low epitope density due to a decrease in the functional affinity of IgM. Studies of binding kinetics showed similar association rates for both molecules. The dissociation rate, however, was slower for IgM at high epitope density and for IgD at low epitope density. Taken together, the results show that IgM and IgD with identical Ag binding regions have different Ag binding properties. ***The Journal of Immunology*****, 2004, 172: 2925–2934.**

The initiation of the humoral immune response involves specific recognition of Ag by the B cell receptor (BCR)[3]. The BCR is comprised of a membrane-bound Ab unit associated with the Ig-α/β heterodimer (1–3). IgD is regarded as the major BCR, coexpressed with IgM on the surface of peripheral mature, naive B cells both in human and mouse (4–6). However, the specific biological role of this BCR coexpression remains elusive despite continuing experimental efforts.

In the periphery, both IgM and IgD binding to Ag can mediate B cell activation and deletion, though putative discrepancies between thymus-independent and thymus-dependent Ags have been observed (7–10). Furthermore, both Igs use essentially the same intracellular signal transduction machinery, but the signals transmitted differ by partly yet unknown mechanisms (11–14).

However, when analyzed in a knockout mouse context both IgD and IgM are to a large extent interchangeable, which points toward a redundancy between IgM and IgD from fetal to adult immune competency (15–17). In contrast, there seems to be a selective advantage for the functional δ allele in heterozygous $IgD^{+/-}$ knockout mice, pointing toward maintenance mechanisms of a dual IgM and IgD function (15). This report also suggests that the IgD-BCR has a role in recruitment of B cells into germinal centers, as the $IgD^{-/-}$ mice exhibited delayed Ab affinity maturation. A recent report further underscores this importance of the IgD-BCR in germinal center development in comparison to the IgM-BCR (14).

Both human and murine IgD have unusually long and Cys-free hinge regions, which may influence the segmental flexibility of their Ag binding sites (18, 19). This has led to the hypothesis that IgD may be more efficient in cross-linking polyvalent Ags than IgM. Indeed, results obtained from cellular assays may indicate that such differences exist (20). However, when further dissecting the putative increased epitope sensitivity observed with the IgD-BCR, it seems only to be a consequence of the higher IgD-BCR expression level on the cells compared with the IgM-BCR (21).

Thus, taken together, the current body of evidence still falls short in clarifying whether or not the IgD and IgM coexpression reflects true genetic redundancy (22). Furthermore, the vast majority of the reports rely on a murine context. In contrast to the other Ab classes, there is poor conservation in the IgD molecule as murine and human IgD have very different primary and probably quaternary structures (19, 23). IgD-like molecules have also been identified in species as evolutionary distant as teleosts, but it seems that there has been a lack of preserving selective pressure, the hallmark of genetic redundancy, when entering the mammalian lineage (24–30).

In this study, we have measured the Ag binding ability of a matched set of soluble chimeric IgM and IgD with specificity for the hapten 5-iodo-4-hydroxy-3-nitrophenacetyl (NIP). All factors other than the differences in the Fab to Fc tether and the Fc itself are thus equalized. This allowed us to analyze functional differences with respect to Ag binding for different epitope densities. Notably, the IgM molecules studied here are H_2L_2 monomers and not the pentamers normally found in the circulation. We have determined both the Fab-Fab flexibility and the intrinsic and functional affinity of these molecules at high and low epitope density. We also compared IgM and IgD with a hinge truncated IgD and chimeric IgG3. For the first time, we here report differences in Ag binding between IgD and IgM harboring identical monovalent specificity. The results show that differences in segmental flexibility and Fab arm reach lead to an epitope density-dependent difference in the

*Department of Molecular Biosciences, University of Oslo, Oslo, Norway; [†]Department of Biological Science and Structural Biology Program, Florida State University, Tallahassee, FL 30306; and [‡]Division of Infectious Disease Control, Norwegian Institute of Public Health, Oslo, Norway

Received for publication July 14, 2003. Accepted for publication December 8, 2003.

The costs of publication of this article were defrayed in part by the payment of page charges. This article must therefore be hereby marked *advertisement* in accordance with 18 U.S.C. Section 1734 solely to indicate this fact.

[1] This work was supported by grants from the Norwegian Cancer Society and the Norwegian Research Council.

[2] Address correspondence and reprint requests to Geir Å. Løset, Department of Molecular Biosciences, University of Oslo, P.O. Box 1041 Blindern, 0316 Oslo, Norway. E-mail address: g.a.loset@bio.uio.no

[3] Abbreviations used in this paper: BCR, B cell receptor; NIP, 5-iodo-4-hydroxy-3-nitrophenacetyl; MS, mass spectroscopy; RU, resonance unit; UH, upper hinge; wt, wild type.

0022-1767/04/$02.00

Ag-binding properties of IgD and IgM. Thus, these differences may have implications for the understanding of the apparent redundancy in biological function of the BCR on mature, naive B cells in a human context.

Materials and Methods

Construction of chimeric IgD molecules

The plasmid vector pAS24 (a gift from Dr. P. W. Tucker, Department of Microbiology, University of Texas Southwestern Medical Center, Dallas, TX) contains a 9.9-kb genomic sequence encoding an incomplete human δ locus in pBR322 (31). Using this plasmid as the initial template, a wild-type (wt) and a h1 exon deletion mutant (Δh1) δ-chain were generated. Gene segments were amplified by PCR using the primer pairs C_H1frwd/H1rev and H2frwd2/C_H3rev for IgD, and C_H1frwd/C_H1rev and H2frwd1/C_H3rev for Δh1 (Table I). Resulting fragments were spliced by overlap extension and amplified using the primers C_H1frwd and C_H3rev. The δ secretory tailpiece was attached to each gene by additional rounds of PCR using the primer pair C_H1frwd/δS. A Gly to Glu substitution in Δh1 was introduced with mismatched bases in the C_H1rev/H2frwd1 primers. Cloned *Pfu* DNA polymerase (Stratagene, La Jolla, CA) was used for primer extension throughout. Both constructs were confirmed by sequencing. The δ constant region genes were ligated into the *Eco*RI/*Bam*HI-digested expression vector pLNOH2 (32) downstream of a V_H domain specific for the hapten NIP (33).

Cell culture and transfections

The δ H chain genes were transfected by electroporation into the murine myeloma cell line J558L (a gift from Dr. S. L. Morrison, Department of Microbiology, Molecular Biology Institute, University of California, Los Angeles, CA). The cells were grown and transfected as described previously (34). Supernatants were screened for NIP-specific Ab production by NIP-BSA sandwich ELISA developed with H chain-specific Abs as described previously (35). The best IgD- and IgDΔh1-producing transfectomas were expanded to a high-density cell culture miniPERM bioreactor (Hereaus, New York, NY). Cell lines producing chimeric IgMC575S (a monomeric IgM) and IgG3, both with NIP specificity, have been described previously (34, 36).

Ab purification and analysis

NIP-specific Abs were purified by affinity chromatography on a 4-hydroxy-3-nitrophenacetyl-coupled AH Sepharose 4B column (Amersham Pharmacia Biotech) and eluted with 30 ml of 0.2 mM NIP in PBS/0.02% azide. After vacuum concentration using a Schleicher & Schüll cartridge (Dassel, Germany), the concentrates were dialyzed against PBS/0.02% azide for 1 wk with several changes of PBS. Protein concentration in the purified material was determined both by quantitative ELISA and UV absorption at 280 nm using an extinction coefficient of 1.4. To verify the absence of noncovalent oligomeric Ig forms comprised by aggregates of H_2L_2 units, samples of 25 μg purified Abs were analyzed by HPLC using a Superdex 200 HR column (Amersham Pharmacia Biotech) in a buffer containing 0.05 M Tris-HCl, 0.2 M NaCl, 2 M EDTA, and 0.02% azide (pH 7.6). The analysis was conducted with a constant flow rate of 0.5 ml/min and a pressure of 6 bar. In addition, the affinity-purified Abs were run on a non-reducing 8% SDS-polyacrylamide gel and blotted onto a polyvinylidene fluoride membrane (Millipore, Bedford, MA) in Tris/glycine buffer (25 mM Tris, 192 mM glycine, and 20% methanol, pH 8.3) at 100 V for 1 h in a Bio-Rad mini-protean II blotting unit. The membrane was blocked with 5% skim milk in PBS for 1 h at room temperature followed by washing with PBS/0.05% Tween 20 (PBS/T). The membrane was developed by incubation with biotinylated anti-mouse λ_1 L chain Ab (Southern Biotechnology Associates, Birmingham, AL) and streptavidin-HRP (Amersham Pharmacia Biotech).

The molecular mass of IgD, IgDΔ1, and IgMC575S were determined by mass spectroscopy (MS) on a Voyager-DE RP mass spectrophotometer (Applied Biosystems, Foster City, CA). Briefly, 1 μl of affinity-purified Ab (0.5–1 mg/ml) was diluted in 10 μl of sinapinic acid and 2 μl was transferred to a grid. The grid was loaded into the instrument after 15 min of air drying and subjected to matrix-assisted laser desorption ionization-time of flight MS analysis.

Both IgD and IgDΔh1 were tested for Jacalin binding in ELISA. Jacalin (Sigma-Aldrich, St. Louis, MO) was adsorbed to microtiter plates (Nunc, Roskilde, Denmark) at 100 μg/ml in PBS (pH 7.4) overnight at 4°C. Control wells with NIP-BSA, prepared as described elsewhere (35), were coated likewise. After washing with PBS/T, 8 nM Ab in PBS/T was allowed to bind for 90 min at room temperature. Ab binding was detected by the addition of biotinylated anti-mouse λ_1 L chain Ab (1/1000) and streptavidin-HRP (1/2000) in PBS/T followed by incubation for 90 min at room temperature. An assay volume of 100 μl/well was used throughout, and the plates were washed five times with PBS/T between each incubation step. The plates were developed by adding 100 μl/well ABTS substrate (0.05 M citric acid, pH 4, with 220 μg/ml diammonium salt) containing 0.2% H_2O_2 and incubating for 10 min at room temperature. The color reaction was measured at 405 nm using a Flow Titertek Multiscan Plus Mk II spectophotometer (ICN, Costa Mesa, CA). Furthermore, a competition ELISA was performed in which a gradient of α-D-melibiose (Sigma-Aldrich) was added to a constant amount of IgD. Briefly, samples containing from 1 to 1000 mM α-D-melibiose in 100 μl of PBS/T were added to 2 nM IgD in 100 μl of PBS/T. These mixtures were then applied on Jacalin-coated wells and Ab binding was detected as described above.

NIP-specific Fab were prepared by dissolving chimeric NIP-specific IgG4 (9 mg/ml) in PBS (pH 7.4) containing 20 mM cysteine and 5 mM EDTA followed by digestion with papain (Sigma-Aldrich) at a papain to IgG4 w/w ratio of 2:100 at 37°C for 16 h. The digested mixture was passed through a protein A-Sepharose column (Amersham Pharmacia Biotech) and Fab was eluted with PBS (pH 7.4). The Fab fraction was further purified by gel filtration through a Superdex 200 column (1 × 30 cm) (Amersham Pharmacia Biotech) and dialyzed against PBS (pH 7.4) overnight.

Immunoelectron microscopy

Immunoelectron microscopic analyses of Abs and immune complexes were performed by negative staining, as described previously (37). Briefly, intact anti-Id IgG and target IgD were mixed at a 1:1 molar ratio (at ~1 mg/ml each) and anti-Id Fab and target IgD were mixed at a 3- to 4-fold molar excess of Fab in borate-buffered saline and incubated at room temperature for 30 min. Following incubation, the reactants were affixed to carbon membranes, stained with uranyl formate, and mounted on copper grids for analysis. Electron micrographs were recorded at × 100,000 magnification on a JEOL CX 1200 electron microscope. Scoring of immune complexes was performed directly on the electron micrographs with a hand-held lens, and angular and hinge length measurements were scored with an optical loupe fitted with a measuring graticule (Electron Microscopy Sciences, Fort Washington, PA). At least 1000 molecules were scored for each sample of intact Id-anti-Id immune complexes and for angular measurements at least 100 molecules were scored for each sample. All

Table I. *Primer sequences utilized to generate IgD and IgDΔh1*

Name	Sequence 5′ → 3′[a]
C_H1frwd[b]	*AGT GGA ATT CC*T CTC GGC AAC AAG AGC CCA GGG
C_H1rev[c]	*CCT CCT CTc tC*T GGC CAG CGG AAG ATC TCC T
H1rev	*CCT CCT CTT* CCT GTG TTA CGG GTG GTG GCT G
H2frwd1[c]	*CGC TGG CCA Gag* AGA GGA GGA GAA GAG AAG AAG
H2frwd2	*CGT AAC ACA GGA* AGA GGA GGA GAA GAG AAG AAG
C_H3rev	*TCT GTT ACA TAG* CTG ACT TCT AGG CTC CGG
δS[d]	*ATA TCG GGA TCC CGA TAG TCA TTT CAT GGG GCC ATG GTC* TGT TAC ATA GCT GAC TTC

[a] Tags are given in italics.
[b] The 5′-end tag contains an *Eco*RI restriction site (underlined) for the subsequent subcloning of the fragment into the pLNOH2 vector.
[c] Lower case letters indicate mismatches.
[d] The 5′-end tag contains most of the δS encoding sequence. In addition, this tag contains a *Bam*HI restriction site (underlined) for the subsequent subcloning of the fragment into the pLNOH2 vector.

scoring was done blind. Only complexes in which both Fab arms were in complex with 5B5 Fab probes and which formed angles between the arms of between 160 and 200° were recorded for measuring of the maximal span that could be bridged by IgD and IgM. The linear measurements between the distal portions of the extended Fab arms were adjusted. This was done by first compensating for the shortened reach in those complexes that deviated from the T-shaped 180° maximal extension and then subtracting the 14 nm contributed by the two attached 5B5 anti-Id Fabs. The distances given represent the average of 25–30 measurements of each molecule.

Thiocyanate elution ELISA

Two different NIP-BSA conjugates with an average of 4 or 15 NIP molecules per BSA molecule, respectively, were prepared essentially as described previously (35). The thiocyanate elution ELISA was performed essentially as described elsewhere (38). The two NIP-BSA conjugates were adsorbed to microtiter plates (Nunc, Roskilde, Denmark) at 1 μg/ml in PBS (pH 7.4) overnight at 4°C. Thus, the epitopes were adsorbed to the surfaces in a random, unspecific manner. However, there is a large difference in the amount of epitopes that are attached to the two surfaces.

Ag integrity after chaotrope exposure was assessed as follows: After blocking residual binding capacity with 5% skim milk, a gradient of ammonium thiocyanate (Sigma-Aldrich) ranging from 0 to 3.0 M in PBS/T were added to NIP-BSA_{15}-coated plates and incubated for 20 min at room temperature. Then, 50 ng IgMC575S in PBS/T was added to each well and incubated for 90 min at 37°C. Ab binding was detected with anti-mouse λ_1 L chain Ab as described above, with the exception that the incubations were done at 37°C. The effect of the chaotrope on the Abs was assessed by mixing 1 μg IgMC575S and IgD, respectively, in 10 μl of PBS with 100 μl of a chaotrope gradient in PBS followed by a 20-min incubation at room temperature. The samples were diluted to total volumes of 3 ml in PBS, transferred to separate dialysis cassettes (Pierce, Rockford, IL), and dialyzed against 1000× volumes of PBS overnight at 4°C. The Ag binding ability was then detected by ELISA as described above.

In the thiocyanate elution ELISA, the Ag binding ability of the Abs was assessed using both Ag conjugates. IgD, IgDΔh1, IgG3, and IgMC575S were added at a concentration previously determined to give an A_{405} of ~1.0 in the NIP-BSA ELISA. Binding was allowed to occur for 90 min at 37°C. Ammonium thiocyanate was then added at concentrations ranging from 0 to 2.0 M in PBS/T, and the plates were incubated for 20 min at room temperature. Ab binding was detected as described above. Functional affinity was displayed as an index corresponding to the molar concentration of ammonium thiocyanate required to produce 50% reduction in Ab binding detected in ELISA. Significant differences ($\alpha \leq 0.05$) were determined using the Wilcoxon rank-sum test.

Surface plasmon resonance analysis

Binding kinetics were determined by surface plasmon resonance using a semiautomatic BIAcore X instrument and the BIAevaluation 3.0 software (Biacore, Uppsala, Sweden). NIP-BSA was immobilized on research grade CM5 sensor chips using the amine coupling kit supplied by the manufacturer. Unreacted moieties on the surface were blocked with ethanolamine. Conjugate concentrations of 300 μg/ml (BSA-NIP_{15}) and 0.5 μg/ml (BSA-NIP_4) in acetate buffer and contact times of 5 min at a flow rate of 5 μl/min gave ~134 resonance units (RU) and 67 RU of immobilized material, respectively. Control BSA surfaces were prepared in an analogous manner. Such random coupling does not allow a controlled distribution of epitopes. Furthermore, the dextran matrix is not a rigid support, but rather behaves as a flexible matrix (39). However, there is a large difference in the amount of hapten that is present on the two chips. Therefore, the BSA-NIP_{15} surface is referred to as the high and the BSA-NIP_4 surface as the low epitope density surface, respectively. HEPES-buffered saline (10 mM HEPES, 150 mM NaCl, 3.4 mM EDTA, and 0.005% surfactant P20, pH 7.4) obtained from the manufacturer was used as sample dilution and running buffer in all experiments. The NIP-specific IgD, IgDΔh1, and IgMC575S were analyzed at 37°C. The kinetic data were examined for mass transport limitations and the flow rates adjusted accordingly. Two different Ab concentrations in a 60-μl volume at a 20-μl/min flow rate were injected (30 nM and 1000 nM) on the low epitope density surface. Likewise, two Ab concentrations (10 and 1000 nM) in a 60-μl volume at a 50-μl/min flow rate were injected on the high epitope density surface. The samples were duplicated and injected in random order. At the end of all runs, the surfaces were regenerated by injecting 10 μl of 50 mM NaOH (pH 12). To minimize interference in the signal at this temperature, the running buffer was preheated to 37°C using a water bath. Likewise, the Ab solutions were heated to 37°C immediately before injection. Four affinity-purified, NIP-specific preparations were analyzed at 25°C, namely, IgD, IgDΔh1, IgG4Fab, and IgMC575S, at concentrations ranging from 20 to 2000 nM. Each sample was duplicated and injected in random order on the low epitope density surface at flow rates between 20 and 50 μl/min. To correct for nonspecific binding and bulk buffer effects, the responses obtained from the control surfaces and blank injections were subtracted from each interaction curve. Kinetic rate constants were calculated simultaneously from the association and dissociation phases of the 25°C interaction curves using predefined models provided by the BIAevaluation 3.0 software. Semiquantitative comparison was performed when analyzing the 37°C runs.

Results

Construction and expression of recombinant NIP- specific Abs

Soluble, full-length chimeric IgD with specificity for the hapten NIP was constructed. The 64-aa structural hinge of human IgD is the longest hinge known to exist in any Ab (19). To dissect how this long hinge affected the binding properties, we created a mutant where the 34 NH_2-terminal hinge amino acid residues were removed by deleting the h1 exon, creating IgDΔh1 (Table II). Due to the splicing pattern, where codons are assembled from neighboring exons, two additional amino acid residues, Glu^{102} and Arg^{137}, would be removed in the exon deletion process and replaced by one Gly residue. Assuming that Glu^{102} could be important for the segmental flexibility (40–42), we chose to reconstitute Glu^{102} by in vitro mutagenesis. The IgMC575S and IgG3 molecules have been described previously (34, 36). The Igs were all expressed in the murine myeloma cell line J558L resulting in identical monovalent specificity due to the H_2L_2 formation with the endogenously expressed λ_1 L chain (33).

Structural analysis

All Igs were affinity purified, analyzed by Western blotting, and found to be secreted as H_2L_2 units (Fig. 1). To compute molar concentrations of IgD, IgDΔh1, and IgMC575S, an accurate molecular mass determination was conducted by MS. The molecular mass of IgD and IgMC575S was estimated to 174.1 and 190.8 kDa, respectively, which are in agreement with previously published results (43–45). As for IgDΔh1, it was found to be 158.8 kDa, which is 15.3 kDa less than the wt molecule. These results are also in accordance with the SDS-PAGE migration patterns observed in Fig. 1. The IgDΔh1 contains a 34-aa deletion, which should reduce the molecular mass by ~6.6 kDa (46). In addition, this region contains four to seven *O*-linked carbohydrate moieties per H chain, which would be absent from the IgDΔh1 (19, 47, 48). The lectin Jacalin binds selectively to α-*O*-glycosides (49) and has been shown to bind endogenous human IgD (50). Thus, to study

Table II. *Hinge region amino acids*

Ig Type	C-terminal C_H1	Upper Hinge
IgD	FRWPE	SPKAQASSVPTAQPQAEGSLAKATTAPATTRNTGRGGEEKKKEKEKEEQEERETKTPE
IgDΔh1	FRWPE	RGGEEKKKEKEKEEQEERETKTPE
IgG3	VDKRV	ELKTPLGDTTHT
IgMC575S	VPLPG	–[a]

[a] IgM does not possess a hinge region but contains an extra Ig domain.

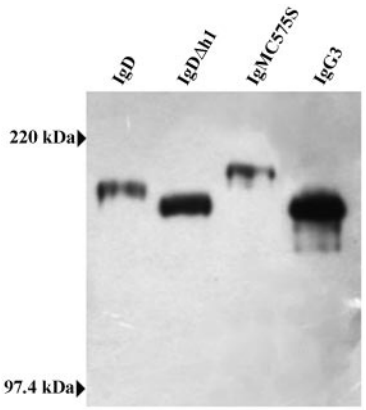

FIGURE 1. Western blot analysis. Affinity-purified Abs were run on a 8% nonreducing SDS-PAGE, blotted onto a polyvinylidene fluoride membrane, and developed using anti-λ_1 L chain Ab as described in *Materials and Methods*.

whether the deletion mutant indeed lacked the *O*-linked carbohydrate, we tested the Abs for Jacalin binding in ELISA (Fig. 2). While IgD bound specifically to Jacalin, IgDΔh1 did not. Both exhibited similar Ag binding capacity (Fig. 2*A*). Furthermore, IgD binding to Jacalin could be inhibited by α-D-melibiose, a monosaccharide that exhibits strong binding to Jacalin (49) (Fig. 2*B*). We therefore conclude that selective binding of IgD to Jacalin is due to *O*-coupled carbohydrates attached to the hinge and that are missing in IgDΔh1.

Electron microscopic analysis of Ig and immune complexes

We have previously used electron microscopy to document two modes of hinge-related shape and flexibility in human IgMC575S, IgE, IgA2, the four IgG subclasses, and several IgG3 hinge mutants (51, 52). In this report, IgD and IgDΔh1 were studied using the same method. In one set of analyses, the Ag binding sites were tagged by reaction with Fab anti-Id so that the angle between the Fab "arms" could be measured. The data are expressed as the mean angle for the particular target Ig and, as a measure of the degree of variability about this mean, we report the SD as a "hinge fold flexibility function." T-shaped molecules would thus have a mean of 180° and Y-shaped molecules with the most upwardly extending (parallel axes) Fab arms would be 0°. In a second set of analyses, the Ig molecules were complexed with complete Ig anti-Id. The ring complex having the fewest components (in this case one Id and one anti-Id, i.e., a ring dimer) is the energetically most favored form (53). Ring dimers will form preferentially if the flexibility of the arms of the reactants is such that the narrow Y shape is allowed or if the molecules are rigid Y shaped. A rigid T shape in contrast will prohibit the formation of ring dimers and the next larger ring (two Ids and two anti-Ids, i.e., ring tetramer) will be favored.

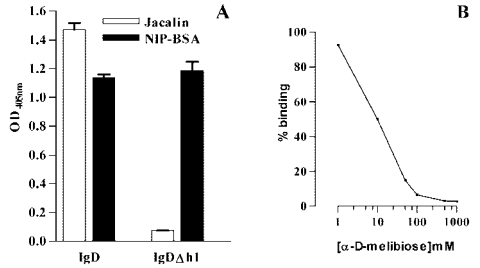

FIGURE 2. *A*, Carbohydrate analysis of IgD and IgDΔh1. The level of Ab binding to Jacalin was measured by ELISA as described in *Materials and Methods*. As control, the Ag binding capacity to NIP-BSA was measured. One of two representative experiments performed in triplicates is shown with the SD indicated by error bars. *B*, Specificity analysis of IgD binding to Jacalin. The ability of α-D-melibiose to compete with IgD for Jacalin binding in ELISA was assessed as described in *Materials and Methods*. Taking Ab binding in the absence of melibiose as 100%, the level of Ab binding as function of melibiose concentration is depicted. The data are representative of two independent experiments.

The results are summarized in Table III, in which previously reported data for chimeric IgG3 and IgMC575S are included for comparison. In addition, representative examples of the various Ig forms are shown in Fig. 3. We show that IgD is the most T shaped on average (142°), on par with what was previously found for IgE (141°) and IgG3 (136°), and by far the most flexible (±77°), exceeding even IgMC575S (±56°). Partial deletion of the hinge in IgD gave a molecule with an average angle midway between T and Y shape (126°) with considerable flexibility (±52°) similar to IgG3 (±53°). IgMC575S was Y shaped in the previous study (105°) and showed a high degree of flexibility (±56°) (52), although clearly less than IgD. We then reacted each Ig with the anti-Id Ab and screened for the ability to form ring complexes of various sizes (52). IgD and IgDΔh1 readily formed ring dimers similar to what had previously been found for IgG3 and approximately one-half of the molecules were seen in this form. However, neither of these molecules could match IgMC575S, which formed 75% ring dimers (52).

Furthermore, we also determined the maximal span that could be bridged by IgD and IgM by linear measurements between the distal portions of the extended Fab arms. The IgD molecule can span a very large distance of 26 ± 2.3 nm, but is closely rivaled by IgM, which can span a distance of 23 ± 1.5 nm.

Relative functional affinity determination by thiocyanate elution ELISA

The relative functional affinity of the anti-NIP Igs was investigated by thiocyanate elution ELISA (38). Results obtained with this assay using hapten Ags have been shown to correlate well with results obtained with other established procedures (54, 55). In the elution assay, 0.1–2.0 M ammonium thiocyanate were used to disrupt the binding of anti-NIP Igs to NIP-BSA. Addition of 2.0 M ammonium thiocyanate reduced the binding of all of the Igs to a minimum, such that no further effect was seen when increasing the ammonium thiocyanate concentration. To investigate how epitope density affected the functional affinity, the assay was performed on two different antigenic surfaces. The functional affinity indices were calculated as the molar concentration ammonium thiocyanate required to produce a 50% reduction in binding as detected at A_{405} (Fig. 4*A*). Importantly, samples from the Ab preparations used were analyzed by HPLC both before and after the ELISA to verify

Table III. *Comparison of Ig isotypes and mutants*

Ig Type	IgD	IgDΔh1	IgMC575S[a]	IgG3[a]
UH length (no. of amino acids)	58	24	NA[b]	12
% ring dimers	51	50	75	47
Mean Fab-Fab angle	142°	126°	105°	136°
Hinge fold flexibility[c]	±77°	±52°	±56°	±53°

[a] The data for IgG3 and IgMC575S have been published previously (51, 52).
[b] NA, Not applicable.
[c] The SD values is taken as a measure of the degree of flexibility (hinge fold flexibility) about the mean angle.

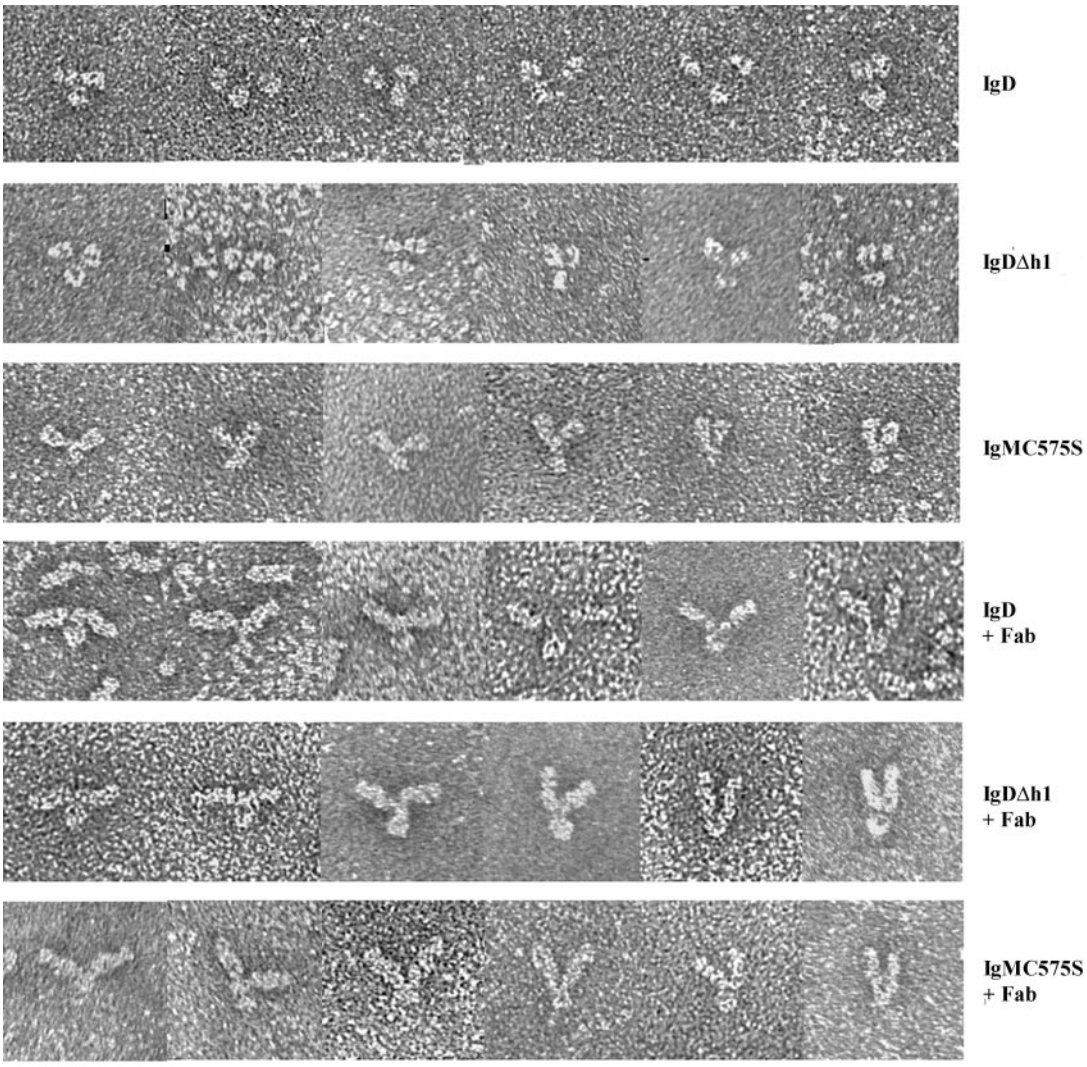

FIGURE 3. Panel of selected electron micrograph images of IgD, IgDΔh1, and IgMC575S with and without attached Fab anti-Id 5B5. The electron micrographs were recorded at ×100,000 magnification.

the complete absence of oligomers comprised by noncovalent H_2L_2 units (data not shown).

Whereas IgD bound with similar functional affinity at both high and low epitope density, the other molecules bound with less strength at low epitope density. IgMC575S was a better binder than IgD at high epitope density (mean, 0.39 M ± 0.02 vs 0.32 M ± 0.06, $n = 8$, $\alpha = 0.029$), whereas IgD was a better binder than IgMC575S at low epitope density (0.32 M ± 0.06 vs 0.23 M ± 0.02, $n = 6$, $\alpha = 0.05$). This was largely due to IgMC575S losing binding strength at low epitope density. There was no significant difference between IgD and IgDΔh1 at high epitope density (0.32 M ± 0.06 vs 0.33 M ± 0.02, $n = 8$). At low epitope density, however, the binding ability of IgDΔh1 decreased some and, consequently, IgDΔh1, on average, bound weaker than its wt counterpart (0.26 M ± 0.04 vs 0.32 M ± 0.06, $n = 6$). On both surfaces IgG3 bound weakest of all of the Igs (0.28 M ± 0.04 and 0.14 M ± 0.02, $n = 5$). Thus, the Ag binding strength of the various Abs could be ranked in the order IgMC575S > IgDΔh1 ≥ IgD > IgG3 at high epitope density, and IgD ≥ IgDΔh1 ≥ IgMC575S > IgG3 at low epitope density, respectively.

To exclude the possibility that the reagents were affected by treatment with the chaotrope, both the anti-NIP Igs and the high-density NIP-BSA preparation were preincubated with ammonium thiocyanate before assessment of Ab binding to Ag. Preincubation was demonstrated not to influence subsequent Ab binding to solid-phase bound NIP-BSA (Fig. 4*B*). However, preincubation of IgD and IgMC575S and subsequent removal of the ion by dialysis decreased the Ag binding capacity weakly, starting at chaotrope concentrations of 0.8 and 0.6 M, respectively (Fig. 4*C*). This may indicate a weak loss of overall molecular integrity from this point forward, which is well above the chaotrope concentrations found in the experiment depicted in Fig. 4*A*.

The effect of epitope density on Ab binding kinetics

To investigate how the H chain regions of the Igs affected the kinetics of the Ag binding process and how the kinetics differed at high and low epitope density, two different antigenic surfaces were generated with BSA-NIP_{15} and BSA-NIP_4. Both Ag preparations were immobilized by random amine coupling on research grade CM5 chips, reaching a level of 67 RU with BSA-NIP_4 and 134 RU with BSA-NIP_{15}, respectively. The conjugation levels were deliberately kept this low because we anticipated that this would enhance our ability to reveal putative differences in Ab binding. The 134 and the 67 RU surfaces were taken to represent high and low epitope density, respectively. A semiquantitative comparison between the binding kinetics at these two epitope densities measured

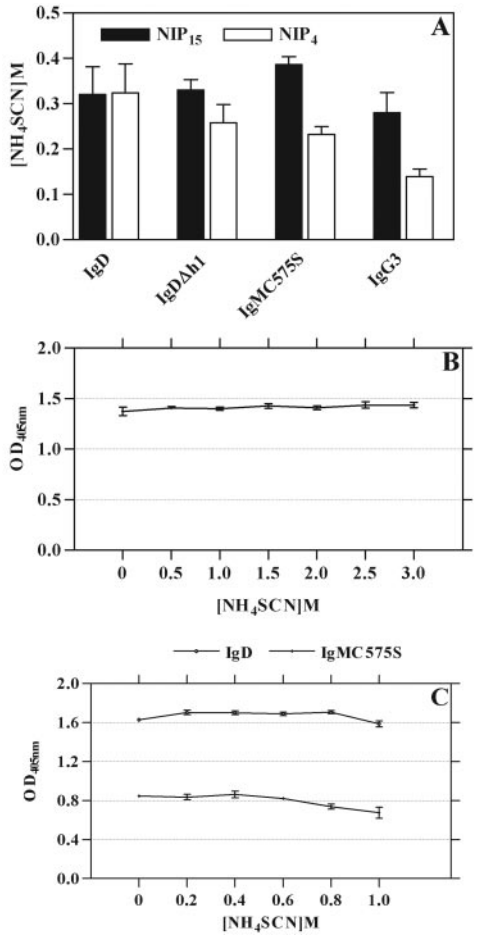

FIGURE 4. *A*, Thiocyanate elution ELISA. Abs in PBS/T were added to microtiter plates with NIP-BSA at high (NIP_{15}) and low (NIP_4) epitope density, respectively, to give an absorbance at 405 nm of ~1.0. A gradient of NH_4SCN was added and the amounts required to reduce binding by 50% are depicted in the histograms. An Ab of irrelevant specificity was included in all of the measurements as negative control (data not shown). The results represent the average of at least three independent measurements with the SD indicated by error bars. *B*, The antigenic integrity after thiocyanate exposure was assessed by the capacity to adsorb Ab. NIP-BSA-coated wells were incubated with a gradient of the chaotrope, followed by IgMC575S binding and detection as described in *Materials and Methods*. One of three representative experiments performed in triplicates is shown with the SD indicated by error bars. *C*, Ab integrity after thiocyanate exposure assessed by the capacity to bind Ag. IgMC575S and IgD were preincubated with a gradient of thiocyanate followed by removal of the chaotrope by dialysis as described in *Materials and Methods*. Remaining Ag binding ability is taken as a measure of structural integrity. One of three representative experiments performed in triplicates is shown with the SD indicated by error bars.

at 37°C was performed using a BIAcore (Fig. 5). The sensorgrams for each molecule were overlaid and the slopes of the association and dissociation curves were compared. To better visualize the shapes of the progress curves and thereby the differences between the data sets, the sensorgram overlays were rescaled to percent response.

The observed association rates of IgMC575S and IgDΔh1 were virtually the same at both 30 nM and 1000 nM concentrations on the low epitope density surface, while IgD exhibited a marginally slower observed association rate. Furthermore, IgD had the slowest observed dissociation phase, followed by IgDΔh1 and then IgMC575S (Fig. 5, *A* and *B*). At high epitope density and at both 1000 and 10 nM concentrations, the observed association rates of IgMC575S, IgD, and IgDΔh1 were similar (Fig. 5, *C* and *D*). However, the observed dissociation rates were opposite from the situation with low epitope density as IgMC575S dissociated slower than IgD and IgDΔh1 (Fig. 5, *C* and *D*).

The intrinsic affinity was derived from the association and dissociation rate constants for an anti-NIP Fab on the low epitope density surface at 25°C. The Fab molecule was purified to homogeneity by size-exclusion chromatography immediately before the analysis. The kinetic rate constants were obtained using a ligand heterogeneity model, which gave the best global fit using the BIAevaluation 3.0 software. As shown in Fig. 6, the Fab exhibited a rapid dissociation. The k_{off} value was 0.12 s^{-1} while the k_{on} value was estimated to 3.32×10^5 $M^{-1}s^{-1}$ (Table IV). An affinity of 3.6×10^{-7} M was derived from the estimated rate constants according to the equation $K_d = k_{off}/k_{on}$. This is supported by results from the high epitope density surface, where the K_d was estimated by equilibrium analysis to a value of 3.0×10^{-7} M (data not shown).

Serial injections of IgMC575S, IgD, and IgDΔh1 were done on the low epitope density surface at 25°C (data not shown). As expected, the data did not fit a simple first-order bimolecular interaction model, since the analytes are bivalent molecules. Consequently, a model attempting to describe bivalent binding kinetics was applied. This model describes the binding of a bivalent analyte to immobilized ligand, where one analyte molecule can bind to one or two ligands. Binding to the first ligand is described by a single set of rate constants, k_{on} and k_{off}, which corresponds to the intrinsic affinities of the various molecules. The derived kinetics is summarized in Table IV. The k_{on} and k_{off} values all fell in a relatively narrow window and yielded K_d values 4- to 8-fold lower than the value obtained for the Fab. This should be expected since the individual Fabs in the context of complete Abs have numerous favorably oriented Fabs in the extreme vicinity of the reaction surface and thus a higher probability of rebinding.

Binding to the second ligand by the same analyte is described by a second set of rate constants, k_{on2} and k_{off2}. IgDΔh1 and IgMC575S were almost indistinguishable, but clearly different from that of IgD. The order is virtually the same as in the qualitative comparison (Fig. 5) and, furthermore, the difference is clear both in the on- and off-rate, as is also clearly visible in Fig. 5, *A* and *B*. Large differences between the derived association rate constants of the three molecules were obtained, ranging from 4.3 to 100.1×10^5 $M^{-1}s^{-1}$, where IgD exhibits the slowest, IgDΔh1 intermediate, and IgMC575S the fastest kinetics. Furthermore, IgD had 10-fold slower k_{off2} than IgDΔh1 and IgMC575S, which suggests that IgD has a higher degree of bivalent binding at low epitope density. Notably, there is a discrepancy between the observed dissociation rate of IgDΔh1, which is similar to that observed for IgMC575S, and the higher k_{off2} value with a very high SEM estimated for IgDΔh1. As in the ELISA, samples from the Ab preparations used in the BIAcore analysis were analyzed by HPLC before and after the assays to verify the complete absence of noncovalent oligomers of H_2L_2 units (data not shown).

Discussion

The role of flexibility and reach in Ab function

In this study, we compare the Ag binding ability of a matched set of Abs with identical binding regions, but with marked differences in the C region, namely, IgM, IgD, and a mutant of IgD with a truncated hinge. The aim of the study was to shed light on an intrinsic functional property of IgD compared with IgM, namely, how differences in segmental flexibility and reach translates into

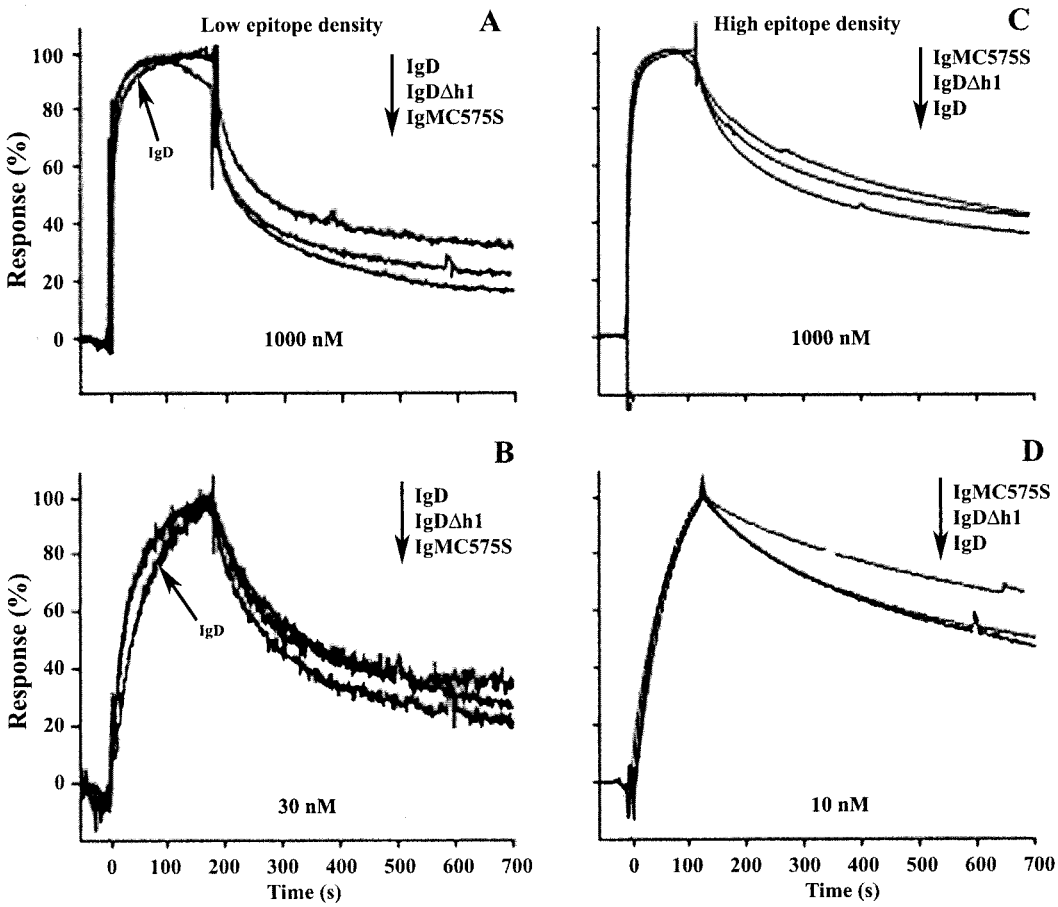

FIGURE 5. Semiquantitative comparison of Ab binding kinetics at high (NIP_{15}) and low (NIP_4) epitope density. The data were rescaled with the maximum response of each sensorgram as 100%. Sensorgram overlays of the 1000 nM (*A*) and the 30 nM (*B*) Ab injection at low epitope density and of the 1000 nM (*C*) and the 10 nM (*D*) Ab injection at high epitope density are given. Deviations in the curves, such as the premature drop in the late association response for one of the Abs in *A*, were caused by disturbances in the reference cell during the injections at 37°C and are a consequence of gas formation in the internal flow system and thus do not reflect the genuine binding event.

their ability to engage Ag at different epitope densities. IgM and IgD are coexpressed as BCRs on mature, naive B cells and play a pivotal role in the initiation of the humoral immune response. The apparent redundancy in BCR expression remains elusive, but structural information may give a lead to their individual roles. We have attempted to equalize all factors other than the differences in the Fab to Fc tether, thus enabling us to measure the functional consequence of the hinges in these molecules. The results presented clearly support the hypothesis that segmental flexibility enhances the ability to bind Ag at low epitope density by allowing unrestricted Fab movement and thereby bivalent binding (56–58). Furthermore, depending on the distance between the epitopes, reach may well be as important as flexibility in determining the feasibility of bivalent binding.

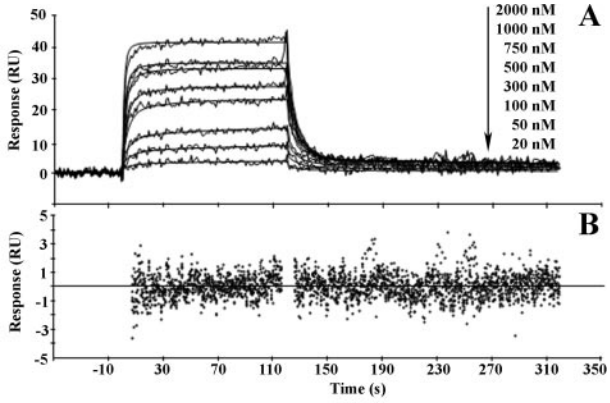

FIGURE 6. *A*, Corrected sensorgram overlays for the NIP-BSA Fab interaction. The fluctuating lines represent repeated injections of Fab ranging from 20 nM to 2 μM. The solid straight lines that intersect the data points are the best global fits to the heterogeneous ligand model using nonlinear least-squares analysis. *B*, Residual plot for the global fit of the experimental vs modeled data shows random distribution at the instrument noise level.

The upper hinge length affects segmental flexibility

The IgD molecule possesses an unusually long and glycosylated structural hinge. Both IgD and IgA1 have hinges that lack the extensive disulfide bridging seen in the other hinge-containing Igs, and both possess *O*-linked carbohydrates. Recently, homology modeling of human IgA1 suggests that its hinge peptides are extended structures, which due to the high incidence of *O*-glycosylation and in the context of the whole Ab yields a T-shaped molecule with almost 180° between the paratopes (59). Thus, the part of the IgD hinge that is glycosylated may be extended as well.

In this study, we show by electron microscopy that IgD on average is T shaped, but is by far the most flexible of all Igs previously tested by this method and can readily form acute Y-shaped angles necessary for ring dimer formation. In accordance with this,

Table IV. *Anti-NIP binding kinetics*[a]

	k_{on} (10^4/Ms)	k_{off} (10^{-3}/s)	k_{on2} (10^5/Ms)[b]	k_{off2} (/s)	χ^{2c}
Fab	33.2 ± 1.5	123.0 ± 3.4	NA[d]	NA[d]	0.7
IgD	6.6 ± 0.1	6.3 ± 0.2	4.3 ± 0.1	0.19 ± 0.01	0.6
IgDΔh1	12.7 ± 0.2	5.7 ± 0.2	64.6 ± 31.6	2.47 ± 1.21	0.7
IgMC575S	10.0 ± 0.1	4.8 ± 0.1	100.1 ± 0.7	2.07 ± 0.02	0.7

[a] Kinetics of Fab, IgD, IgDΔh1, and IgMC575S binding to NIP-BSA calculated by global analysis on the low epitope density surface using a heterogeneous ligand (Fab) and a bivalent (Abs) interaction model. The analysis was conducted at 25°C and all values are given ± SEM.
[b] k_{on2} (RUs^{-1}) to k_{on2} ($M^{-1}s^{-1}$): k_{on2} × molecular mass × 100.
[c] Chi square values resulting from global curve fitting using nonlinear least-squares analysis.
[d] NA, Not applicable.

the IgD molecule can easily accommodate a closed ring dimer conformation. Thus, it is clear that even though the upper hinge (UH) is heavily glycosylated, there appears to be little steric hindrance due to carbohydrate clustering. The UH is defined as the peptide that stretches from the end of C_H1 to the first Cys residue in the hinge that forms an inter-H chain disulfide bond (60). Such a constraint could potentially lock the individual Fab arms of the molecule in a narrow window of permissive conformations, which is clearly not the case. The IgDΔh1 mutant has 24 aa in the UH and lacks carbohydrate altogether. Electron microscopy shows that it is less T shaped and has lower hinge fold flexibility than its wt counterpart. This may relate to the reduced length of the hinge, the lack of carbohydrate, or both. The IgDΔh1 behaves roughly similar to IgG3 with its 12 aa and unglycosylated UH. IgMC575S has been described previously (52). Compared with IgD, IgMC575S is more Y shaped and has lower hinge fold flexibility. Nevertheless, it is better able to form ring dimers than IgD and IgDΔh1. We have previously suggested that the mean Y shape of the molecule might predispose the Fab arms into a geometry that favors cross-linking and ring dimer formation (52).

The 26-nm distance bridgeable by the Fabs of a single monomeric Ab molecule identified for the IgD molecule is, to our knowledge, the largest distance reported to date (61). This suggests that IgD is able to bind bivalently to Ag molecules with epitopes separated by a larger distance than any other Ab.

Affinity discrimination measured by relative functional affinity

In light of the flexibility data, we wanted to study whether or not there is a functional consequence associated with the differences in segmental flexibility. In the solid-phase ELISA, we obtained relative values for the functional affinity of IgD, IgDΔh1, IgMC575S, and IgG3. These values are comparable given the identical experimental conditions. The matched set of anti-NIP Abs was tested on two different antigenic surfaces, which represented high and low epitope density, respectively, and the corresponding functional affinities were ranked. Functional affinity corresponds to the concentration of ammonium thiocyanate required to reduce Ab binding by 50%. The possibility that the bound NIP-BSA antigenic complex is affected by treatment with this chaotropic reagent has been tested in a previous study (55), where it was shown that preincubation with ammonium thiocyanate did not affect subsequent Ab binding. In the present study, we confirmed this finding. Furthermore, we also show that the Ab integrity is unaffected by the chaotrope in the concentration range where the 50% inhibition takes place and, thus, these values can be adequately taken as measure solely of the strength of the binding between the immune complexes.

Given identical specificity and no steric binding constraints, one would expect that the Ab molecule with the least segmental flexibility would be the better binder, as the loss of entropy should be minimized. On the high epitope density surface, we found that IgMC575S bound better than the IgD molecule, which, in turn, bound about as well as the IgDΔh1 molecule. This is in accordance with what was observed in electron microscopy where IgMC575S made ring dimers more readily than the other subclasses. IgDΔh1 has decreased reach and hinge fold flexibility compared with IgD. However, this did not impair binding to the high epitope density surface.

On the low epitope density surface, IgD was the better binder, followed by IgDΔh1, while IgMC575S binding was reduced >40% of that observed at high epitope density. This indicates that the limited reach and/or flexibility of IgM reduced its ability for bivalent binding at the low epitope density surface, whereas IgD bound both surfaces equally well. The difference in functional affinity that appeared between IgD (58 aa UH) and IgDΔh1 (24 aa UH) at low epitope density surface is most likely caused by the loss of reach and/or flexibility of the Δh1 version as compared with the IgD molecule.

When comparing IgG3 (12 aa UH) with IgD and IgDΔh1, only minor differences in binding strength were observed at high epitope density. On this surface, the reach of the Fab arms seems to be of little importance, as long as it is sufficient to provide the opportunity for bivalent binding. In contrast, the results at the low epitope density surface suggest that the reach and hinge flexibility are the dominant parameters with respect to functional affinity. IgD was the best binder and the difference between this molecule and IgG3 was pronounced.

Kinetic aspects of bivalence

Two different Ag surfaces comparable to those in the solid-phase ELISA were generated, and the effects of different epitope density on the Ab-Ag-binding kinetics were assessed by surface plasmon resonance. A semiquantitative comparison of the obtained sensorgrams exhibited the same trend in binding kinetics as the solid-phase ELISA. Thus, we found that the binding strength to NIP of IgMC575S, IgDΔh1, and IgD at high epitope density could be ranked in this order, with IgMC575S most tightly bound. This result again argues that entropy effects, and not reach, are the determining factor at high epitope density. At low epitope density, the binding strength is ranked in the opposite order. This result is also in concordance with previous arguments that on the low epitope density surface, reach and/or flexibility provided by the long UH are contributing as major factors in allowing bivalence and thereby a stable Ab-Ag complex (41, 42, 52, 62).

Discrepancies between intrinsic and functional affinity

The intrinsic association and dissociation rate constants for IgD, IgDΔh1, IgMC575S, and a corresponding monomeric IgG4 Fab were tentatively determined by fitting data obtained on the low

epitope density surface. The low epitope density surface was chosen, as low ligand density makes it less likely that rebinding occurs. Small differences in intrinsic kinetics (k_{on} and k_{off}) between the three complete Abs were observed. However, rate constants describing the cooperative binding step (k_{on2} and k_{off2}) differed such that IgMC575S had 23-fold faster association than IgD. This refers to the binding of the second Fab arm after the first has already bound. Obviously, this will be slower for the more flexible IgD, as Fabs in the context of the IgD hinge most likely diffuse through a larger volume before binding than Fabs in the context of IgMC575S. Furthermore, the k_{off2} rates differ by a factor of 10, with IgD having the slowest off rate.

Clearly, the bivalent model used in this study is too simplistic to describe all of the components of the true interaction (63). This is particularly evident when observing the higher k_{off2} value estimated for IgDΔh1 as opposed to the observed dissociation kinetics. To give a more complete kinetic description, parameters such as the functional difference between the two binding sites on the analyte, ligand density, and steric hindrance must be incorporated in the model (63, 64). Furthermore, even a lower epitope density would have been necessary to minimize rebinding of Fab arms of IgD, where the flexibility and reach is great. This emphasizes the classical problem in studying bivalent binding. Nevertheless, the results from both the ELISA and the BIAcore exhibited the same affinity discrimination between high and low epitope density surfaces.

The results presented in this work strongly indicate that IgD and IgM have different Ag binding modes with respect to different epitope densities. IgM forms a more stable Ab-Ag complex than IgD at high epitope density, while the situation is reversed at low epitope density. This is related to differences in their molecular structure and, in particular, the segmental flexibility required for unrestricted Fab movement. We chose to investigate the molecules in solution. In vivo, soluble IgM exerts its function mainly as pentameric units while we used a monomeric unit. Clearly, the polymeric IgM molecules would exceed the monomeric IgD with respect to functional affinity and reach (44, 65). However, it has been shown that the BCR exists as preformed oligomers and aggregates in lipid rafts upon Ag binding (66, 67). Despite this surface multivalence, depending on the form in which the Ag is encountered, the binding strength of the BCR toward its Ag greatly affects the level of a resulting T cell activation (68–70). Thus, our results may have implications for the apparent redundancy in BCR expression on mature, naive B cells in a human context. In light of the results provided, it seems as though IgD and IgM coexpression rather represents a BCR degeneracy, in which the two slightly different molecules occupy different, but overlapping functions (71). Thus, together they may make a given B cell able to respond more efficiently to a larger range of pathogens ensuring increased survival of the organism. Although we do not provide data that show discrepancies in cellular response associated with the difference in the Ag binding capacity reported, we do for the first time provide molecular data to show that there is indeed an inherent difference in Ag binding between the two forms of the BCR, IgM and IgD. By selecting the appropriate Ags for further analysis, such cellular differences may very well be revealed.

Acknowledgments

We are grateful to Drs. Ole H. Brekke, John E. Stacy, and Stig Omholdt for helpful discussions and Prof. Brian Sutton for critical reading of this manuscript. We also thank Randi Sandin for excellent technical assistance and Prof. Tom Kristensen for conducting the MS analysis.

References

1. Wienands, J., J. Hombach, A. Radbruch, C. Riesterer, and M. Reth. 1990. Molecular components of the B cell antigen receptor complex of class IgD differ partly from those of IgM. *EMBO J. 9:449.*
2. Hombach, J., T. Tsubata, L. Leclercq, H. Stappert, and M. Reth. 1990. Molecular components of the B-cell antigen receptor complex of the IgM class. *Nature 343:760.*
3. Campbell, K. S., and J. C. Cambier. 1990. B lymphocyte antigen receptors (mIg) are non-covalently associated with a disulfide linked, inducibly phosphorylated glycoprotein complex. *EMBO J. 9:441.*
4. Salsano, F., S. S. Froland, J. B. Natvig, and T. E. Michaelsen. 1974. Same idiotype of B-lymphocyte membrane IgD and IgM: formal evidence for monoclonality of chronic lymphocytic leukemia cells. *Scand. J. Immunol. 3:841.*
5. Goding, J. W., and J. E. Layton. 1976. Antigen-induced co-capping of IgM and IgD-like receptors on murine B cells. *J. Exp. Med. 144:857.*
6. Havran, W. L., D. L. DiGiusto, and J. C. Cambier. 1984. mIgM:mIgD ratios on B cells: mean mIgD expression exceeds mIgM by 10-fold on most splenic B cells. *J. Immunol. 132:1712.*
7. Cambier, J. C., F. S. Ligler, J. W. Uhr, J. R. Kettman, and E. S. Vitetta. 1978. Blocking of primary in vitro antibody responses to thymus-independent and thymus-dependent antigens with antiserum specific for IgM or IgD. *Proc. Natl. Acad. Sci. USA 75:432.*
8. Marshall-Clarke, S., K. D. Keeler, and M. E. Parkhouse. 1983. The expression of surface IgD on B cells responsive to thymus-independent and thymus-dependent antigens and its requirement for B-cell triggering. *Immunology 48:393.*
9. Brink, R., C. C. Goodnow, J. Crosbie, E. Adams, J. Eris, D. Y. Mason, S. B. Hartley, and A. Basten. 1992. Immunoglobulin M and D antigen receptors are both capable of mediating B lymphocyte activation, deletion, or anergy after interaction with specific antigen. *J. Exp. Med. 176:991.*
10. Brink, R., C. C. Goodnow, and A. Basten. 1995. IgD expression on B cells is more efficient than IgM but both receptors are functionally equivalent in upregulation CD80/CD86 co-stimulatory molecules. *Eur. J. Immunol. 25:1980.*
11. Venkitaraman, A. R., G. T. Williams, P. Dariavach, and M. S. Neuberger. 1991. The B-cell antigen receptor of the five immunoglobulin classes. *Nature 352:777.*
12. Kim, K. M., and M. Reth. 1995. The B cell antigen receptor of class IgD induces a stronger and more prolonged protein tyrosine phosphorylation than that of class IgM. *J. Exp. Med. 181:1005.*
13. Reth, M. 2001. Oligomeric antigen receptors: a new view on signaling for the selection of lymphocytes. *Trends Immunol. 22:356.*
14. Chaturvedi, A., Z. Siddiqui, F. Bayiroglu, and K. V. Rao. 2002. A GPI-linked isoform of the IgD receptor regulates resting B cell activation. *Nat. Immunol. 3:951.*
15. Roes, J., and K. Rajewsky. 1993. Immunoglobulin D (IgD)-deficient mice reveal an auxiliary receptor function for IgD in antigen-mediated recruitment of B cells. *J. Exp. Med. 177:45.*
16. Nitschke, L., M. H. Kosco, G. Kohler, and M. C. Lamers. 1993. Immunoglobulin D-deficient mice can mount normal immune responses to thymus-independent and -dependent antigens. *Proc. Natl. Acad. Sci. USA 90:1887.*
17. Lutz, C., B. Ledermann, M. H. Kosco-Vilbois, A. F. Ochsenbein, R. M. Zinkernagel, G. Kohler, and F. Brombacher. 1998. IgD can largely substitute for loss of IgM function in B cells. *Nature 393:797.*
18. Tucker, P. W., C. P. Liu, J. F. Mushinski, and F. R. Blattner. 1980. Mouse immunoglobulin D: messenger RNA and genomic DNA sequences. *Science 209:1353.*
19. Takahashi, N., D. Tetaert, B. Debuire, L. C. Lin, and F. W. Putnam. 1982. Complete amino acid sequence of the delta heavy chain of human immunoglobulin D. *Proc. Natl. Acad. Sci. USA 79:2850.*
20. Pure, E., and E. S. Vitetta. 1980. The murine B cell response to TNP-polyacrylamide beads: the relationship between the epitope density of the antigen and the requirements for T cell help and surface IgD. *J. Immunol. 125:420.*
21. Tisch, R., M. Watanabe, M. Letarte, and N. Hozumi. 1987. Assessment of antigen-specific receptor function of surface immunoglobulin M and D with identical hapten specificity. *Proc. Natl. Acad. Sci. USA 84:3831.*
22. Nowak, M. A., M. C. Boerlijst, J. Cooke, and J. M. Smith. 1997. Evolution of genetic redundancy. *Nature 388:167.*
23. Koop, B. F., J. E. Richards, T. D. Durfee, J. Bansberg, J. Wells, A. C. Gilliam, H. L. Chen, A. Clausell, P. W. Tucker, and F. R. Blattner. 1996. Analysis and comparison of the mouse and human immunoglobulin heavy chain J_H-Cμ-Cδ locus. *Mol. Phylogenet. Evol. 5:33.*
24. Ruddick, J. H., and G. A. Leslie. 1977. Structure and biologic functions of human IgD. XI. Identification and ontogeny of a rat lymphocyte immunoglobulin having antigenic cross-reactivity with human IgD. *J. Immunol. 118:1025.*
25. Sire, J., A. Colle, and A. Bourgois. 1979. Identification of an IgD-like surface immunoglobulin on rabbit lymphocytes. *Eur. J. Immunol. 9:13.*
26. Wilson, M., E. Bengten, N. W. Miller, L. W. Clem, L. Du Pasquier, and G. W. Warr. 1997. A novel chimeric Ig heavy chain from a teleost fish shares similarities to IgD. *Proc. Natl. Acad. Sci. USA 94:4593.*
27. Naessens, J. 1997. Surface Ig on B lymphocytes from cattle and sheep. *Int. Immunol. 9:349.*
28. Hordvik, I., J. Thevarajan, I. Samdal, N. Bastani, and B. Krossoy. 1999. Molecular cloning and phylogenetic analysis of the Atlantic salmon immunoglobulin D gene. *Scand. J. Immunol. 50:202.*
29. Stenvik, J., and T. O. Jorgensen. 2000. Immunoglobulin D (IgD) of Atlantic cod has a unique structure. *Immunogenetics 51:452.*
30. Zhao, Y., I. Kacskovics, Q. Pan, D. A. Liberles, J. Geli, S. K. Davis, H. Rabbani, and L. Hammarstrom. 2002. Artiodactyl IgD: the missing link. *J. Immunol. 169:4408.*

31. Word, C. J., M. B. White, W. A. Kuziel, A. L. Shen, F. R. Blattner, and P. W. Tucker. 1989. The human immunoglobulin Cμ-Cδ locus: complete nucleotide sequence and structural analysis. *Int. Immunol. 1:296*.
32. Norderhaug, L., T. Olafsen, T. E. Michaelsen, and I. Sandlie. 1997. Versatile vectors for transient and stable expression of recombinant antibody molecules in mammalian cells. *J. Immunol. Methods 204:77*.
33. Neuberger, M. S. 1983. Expression and regulation of immunoglobulin heavy chain gene transfected into lymphoid cells. *EMBO J. 2:1373*.
34. Sorensen, V., I. B. Rasmussen, L. Norderhaug, I. Natvig, T. E. Michaelsen, and I. Sandlie. 1996. Effect of the IgM and IgA secretory tailpieces on polymerization and secretion of IgM and IgG. *J. Immunol. 156:2858*.
35. Michaelsen, T. E., A. Aase, C. Westby, and I. Sandlie. 1990. Enhancement of complement activation and cytolysis of human IgG3 by deletion of hinge exons. *Scand. J. Immunol. 32:517*.
36. Sandlie, I., A. Aase, C. Westby, and T. E. Michaelsen. 1989. C1q binding to chimeric monoclonal IgG3 antibodies consisting of mouse variable regions and human constant regions with shortened hinge containing 15 to 47 amino acids. *Eur. J. Immunol. 19:1599*.
37. Roux, K. H. 1996. Negative-stain immunoelectron-microscopic analysis of small macromolecules of immunologic significance. *Methods 10:247*.
38. Pullen, G. R., M. G. Fitzgerald, and C. S. Hosking. 1986. Antibody avidity determination by ELISA using thiocyanate elution. *J. Immunol. Methods 86:83*.
39. Cunningham, B. C., and J. A. Wells. 1993. Comparison of a structural and a functional epitope. [Published erratum appears in *1994 J. Mol. Biol. 237:513*.] *J. Mol. Biol. 234:554*.
40. Marquart, M., J. Deisenhofer, R. Huber, and W. Palm. 1980. Crystallographic refinement and atomic models of the intact immunoglobulin molecule Kol and its antigen-binding fragment at 3.0 Å and 1.0 Å resolution. *J. Mol. Biol. 141:369*.
41. Schneider, W. P., T. G. Wensel, L. Stryer, and V. T. Oi. 1988. Genetically engineered immunoglobulins reveal structural features controlling segmental flexibility. *Proc. Natl. Acad. Sci. USA 85:2509*.
42. Kim, H., C. Matsunaga, A. Yoshino, K. Kato, and Y. Arata. 1994. Dynamical structure of the hinge region of immunoglobulin G as studied by 13C nuclear magnetic resonance spectroscopy. *J. Mol. Biol. 236:300*.
43. Ishioka, N., N. Takahashi, and F. W. Putnam. 1987. Analysis of the mechanism, rate, and sites of proteolytic cleavage of human immunoglobulin D by high-pressure liquid chromatography. *Proc. Natl. Acad. Sci. USA 84:61*.
44. Perkins, S. J., A. S. Nealis, B. J. Sutton, and A. Feinstein. 1991. Solution structure of human and mouse immunoglobulin M by synchrotron X-ray scattering and molecular graphics modelling: a possible mechanism for complement activation. *J. Mol. Biol. 221:1345*.
45. Shin, S. U., C. F. Wei, A. R. Amin, G. J. Thorbecke, and S. L. Morrison. 1992. Structural and functional properties of mouse-human chimeric IgD. *Hum. Antib. Hybrid. 3:65*.
46. Sambrook, J., E. F. Fritsch, and T. Maniatis. 1989. Appendix D: codons and amino acids. In *Molecular Cloning: A Laboratory Manual*, Vol. 3. N. Ford, C. Nolan, and M. Ferguson, eds. Cold Spring Harbor Lab. Press, New York, p. D. 2.
47. Takayasu, T., S. Suzuki, F. Kametani, N. Takahashi, T. Shinoda, T. Okuyama, and E. Munekata. 1982. Amino acid sequence of galactosamine-containing glycopeptides in the hinge region of a human immunoglobulin D. *Biochem. Biophys. Res. Commun. 105:1066*.
48. Mellis, S. J., and J. U. Baenziger. 1983. Structures of the *O*-glycosidically linked oligosaccharides of human IgD. *J. Biol. Chem. 258:11557*.
49. Kabir, S. 1998. Jacalin: a jackfruit (*Artocarpus heterophyllus*) seed-derived lectin of versatile applications in immunobiological research. *J. Immunol. Methods 212:193*.
50. Aucouturier, P., E. Mihaesco, C. Mihaesco, and J. L. Preud'homme. 1987. Characterization of Jacalin, the human IgA and IgD binding lectin from jackfruit. *Mol. Immunol. 24:503*.
51. Roux, K. H., L. Strelets, and T. E. Michaelsen. 1997. Flexibility of human IgG subclasses. *J. Immunol. 159:3372*.
52. Roux, K. H., L. Strelets, O. H. Brekke, I. Sandlie, and T. E. Michaelsen. 1998. Comparisons of the ability of human IgG3 hinge mutants, IgM, IgE, and IgA2, to form small immune complexes: a role for flexibility and geometry. *J. Immunol. 161:4083*.
53. Murphy, R. M., R. A. Chamberlin, P. Schurtenberger, C. K. Colton, and M. L. Yarmush. 1990. Size and structure of antigen-antibody complexes: thermodynamic parameters. *Biochemistry 29:10889*.
54. Macdonald, R. A., C. S. Hosking, and C. L. Jones. 1988. The measurement of relative antibody affinity by ELISA using thiocyanate elution. *J. Immunol. Methods 106:191*.
55. McCloskey, N., M. W. Turner, and T. D. Goldblatt. 1997. Correlation between the avidity of mouse-human chimeric IgG subclass monoclonal antibodies measured by solid-phase elution ELISA and biospecific interaction analysis (BIA). *J. Immunol. Methods 205:67*.
56. Cooper, L. J., A. R. Shikhman, D. D. Glass, D. Kangisser, M. W. Cunningham, and N. S. Greenspan. 1993. Role of heavy chain constant domains in antibody-antigen interaction: apparent specificity differences among streptococcal IgG antibodies expressing identical variable domains. *J. Immunol. 150:2231*.
57. Cooper, L. J., D. Robertson, R. Granzow, and N. S. Greenspan. 1994. Variable domain-identical antibodies exhibit IgG subclass-related differences in affinity and kinetic constants as determined by surface plasmon resonance. *Mol. Immunol. 31:577*.
58. McCloskey, N., M. W. Turner, P. Steffner, R. Owens, and D. Goldblatt. 1996. Human constant regions influence the antibody binding characteristics of mouse-human chimeric IgG subclasses. *Immunology 88:169*.
59. Boehm, M. K., J. M. Woof, M. A. Kerr, and S. J. Perkins. 1999. The Fab and Fc fragments of IgA1 exhibit a different arrangement from that in IgG: a study by X-ray and neutron solution scattering and homology modelling. *J. Mol. Biol. 286:1421*.
60. Burton, D. R. 1985. Immunoglobulin G: functional sites. *Mol. Immunol. 22:161*.
61. Woof, J. M. 2002. The human IgA-Fc alpha receptor interaction and its blockade by streptococcal IgA-binding proteins. *Biochem. Soc. Trans. 30:491*.
62. Dangl, J. L., T. G. Wensel, S. L. Morrison, L. Stryer, L. A. Herzenberg, and V. T. Oi. 1988. Segmental flexibility and complement fixation of genetically engineered chimeric human, rabbit and mouse antibodies. *EMBO J. 7:1989*.
63. Muller, K. M., K. M. Arndt, and A. Pluckthun. 1998. Model and simulation of multivalent binding to fixed ligands. *Anal. Biochem. 261:149*.
64. Crothers, D. M., and H. Metzger. 1972. The influence of polyvalency on the binding properties of antibodies. *Immunochemistry 9:341*.
65. Rheinnecker, M., C. Hardt, L. L. Ilag, P. Kufer, R. Gruber, A. Hoess, A. Lupas, C. Rottenberger, A. Pluckthun, and P. Pack. 1996. Multivalent antibody fragments with high functional affinity for a tumor-associated carbohydrate antigen. *J. Immunol. 157:2989*.
66. Schamel, W. W., and M. Reth. 2000. Monomeric and oligomeric complexes of the B cell antigen receptor. *Immunity 13:5*.
67. Pierce, S. K. 2002. Lipid rafts and B-cell activation. *Nat. Rev. Immunol. 2:96*.
68. Batista, F. D., and M. S. Neuberger. 1998. Affinity dependence of the B cell response to antigen: a threshold, a ceiling, and the importance of off-rate. *Immunity 8:751*.
69. Batista, F. D., and M. S. Neuberger. 2000. B cells extract and present immobilized antigen: implications for affinity discrimination. *EMBO J. 19:513*.
70. Batista, F. D., D. Iber, and M. S. Neuberger. 2001. B cells acquire antigen from target cells after synapse formation. *Nature 411:489*.
71. Edelman, G. M., and J. A. Gally. 2001. Degeneracy and complexity in biological systems. *Proc. Natl. Acad. Sci. USA 98:13763*.